

Microscopic origin of the magnetic easy-axis switching in Fe_3GaTe_2 under pressure

Jiaqi Li¹, Shuyuan Liu², Chongze Wang^{1,2}, Fengzhu Ren¹, Bing Wang^{1*}, and Jun-Hyung Cho^{1,2*}
¹*Joint Center for Theoretical Physics, School of Physics and Electronics, Henan University, Kaifeng 475004, China*
²*Department of Physics and Research Institute for Natural Science, Hanyang University, 222 Wangsimni-ro, Seongdong-Ku, Seoul 04763, Republic of Korea*
(Dated: October 2, 2025)

The two-dimensional layered ferromagnet Fe_3GaTe_2 , composed of a Te–Fe_I–Fe_{II}/Ga–Fe_I–Te stacking sequence, hosts two inequivalent Fe sites and exhibits a high Curie temperature and strong out-of-plane magnetic anisotropy, making it a promising platform for spintronic applications. Recent experiments have observed a pressure-induced switching of the magnetic easy axis from out-of-plane to in-plane near 10 GPa, though its microscopic origin remains unclear. Here, we employ first-principles calculations to investigate the pressure dependence of the magnetocrystalline anisotropy energy in Fe_3GaTe_2 . Our results reveal a clear easy-axis switching at a critical pressure of approximately 10 GPa, accompanied by a sharp decrease in the magnetic moments arising from Fe_I and Fe_{II} atoms. As pressure increases, spin-up and spin-down bands broaden and shift oppositely due to band dispersion effects, leading to a reduction in net magnetization. Simultaneously, the SOC contribution from Fe_I, which initially favors an out-of-plane easy axis, diminishes and ultimately changes sign, thereby promoting in-plane anisotropy. The SOC contribution from the outer-layer Te atoms also decreases steadily with pressure, although it retains its original sign; this additional reduction further reinforces the in-plane magnetic easy axis. In contrast, Fe_{II} atoms continue to favor an out-of-plane orientation, but their contribution is insufficient to counterbalance the dominant in-plane preference at high pressure. These findings elucidate the origin of magnetic easy-axis switching in Fe_3GaTe_2 and provide insights for tuning magnetic anisotropy in layered materials for spintronic applications.

I. INTRODUCTION

In recent years, two-dimensional (2D) van der Waals (vdW) magnetic materials have attracted growing interest in spintronics owing to their intrinsic spin-dependent properties and highly tunable magnetic ordering. The discovery of intrinsic ferromagnetism in several 2D vdW compounds, including CrI_3 [1], $\text{Cr}_2\text{Ge}_2\text{Te}_6$ [2], Fe_3GeTe_2 [3], Fe_5GeTe_2 [4], Fe_3GaTe_2 [5], VSe_2 [6], MnSe_2 [7], CrSe_2 [8] and CrTe_2 [9] has opened up new opportunities for exploring low-dimensional magnetism and associated spin transport phenomena. Unlike their three-dimensional counterparts, 2D vdW magnets allow for effective control of magnetic properties through external stimuli such as carrier doping, layer thickness, mechanical strain, and hydrostatic pressure. This high tunability makes them ideal platforms for next-generation spintronic, spin-caloritronic, magneto-optical, and quantum information devices, where precise modulation of magnetic states is crucial. [10, 11]

Recently, Zhang *et al.* [5] successfully synthesized high-quality Fe_3GaTe_2 single crystals via the self-flux method and reported a record-high Curie temperature (T_c) of approximately 350–380 K among vdW layered ferromagnets, significantly surpassing that of the widely studied sister compound Fe_3GeTe_2 [3]. Beyond its elevated T_c , Fe_3GaTe_2 exhibits remarkable magnetic characteristics, including strong perpendicular magnetocrystalline anisotropy, a large saturation magnetic moment, and a sizable anomalous Hall angle, all of which persist above room temperature. Among these properties, magnetic anisotropy is particularly important for information storage technologies, as it enhances thermal stability, increases data density, and reduces power consumption, which are key factors for the development of next-generation spin-

tronic and magnetic memory devices [12, 13]. More recently, pressure-dependent measurements have revealed a sharp re-orientation of the magnetic anisotropy in Fe_3GaTe_2 , where the magnetic easy axis switches from out-of-plane to in-plane within the pressure range of 10.3–12.2 GPa [14]. This transition has been tentatively attributed to a competition between interlayer and intralayer exchange interactions, along with an increased density of states near the Fermi level (E_F) under pressure [14]. However, the microscopic mechanism underlying this anisotropy switching remains unresolved. Understanding the origin of this pressure-induced transition is crucial for elucidating the interplay among lattice structure, electronic states, and spin-orbit coupling (SOC). Such insights are essential not only for advancing fundamental knowledge but also for enabling the rational design of 2D magnetic materials with tunable anisotropy. In this study, we address this issue by performing systematic first-principles calculations to uncover the microscopic origin of the magnetic anisotropy transition in Fe_3GaTe_2 under pressure.

In this work, we perform first-principles density functional theory (DFT) calculations to investigate the evolution of the magnetic anisotropy energy (MAE) in Fe_3GaTe_2 under hydrostatic pressure ranging from 0 to 20 GPa. Our calculations reveal a clear spin reorientation transition of the magnetic easy axis from out-of-plane to in-plane at a critical pressure of approximately 10 GPa, consistent with experimental observations [14]. As pressure increases, we also find electronic band broadening, which leads to opposite shifts in the spin-up and spin-down bands and a marked decrease in magnetization near 10 GPa. At the same time, SOC contributions from inequivalent atomic sites exhibit distinct pressure-dependent behavior. For Fe_I atoms in the outer layers, the initially out-of-plane-favoring anisotropy weakens with increasing pres-

sure and eventually reverses to support in-plane alignment. Te atoms at the top and bottom of the vdW structure exhibit a similar decreasing trend in their SOC effect, though without a sign change, thereby further reinforcing the in-plane magnetic preference. In contrast, Fe_{II} atoms in the central layer retain a weak out-of-plane preference, but their contribution remains too small to counterbalance the dominant in-plane-driving effects from Fe_I and Te at high pressure. These atom-resolved insights clarify the microscopic origin of the pressure-induced magnetic anisotropy transition in Fe₃GaTe₂, highlighting the interplay between electronic band evolution and site-specific SOC effects. Our findings demonstrate that pressure offers an effective route to modulate magnetic anisotropy in 2D vdW magnets, providing useful guidance for the design of spintronic devices with controllable magnetic functionality.

II. CALCULATIONAL METHODS

Our first-principles DFT calculations were performed using the Vienna *ab initio* simulation package (VASP) [15, 16] with a plane-wave basis set. The interactions between core and valence electrons were treated using the projector augmented-wave (PAW) method [17]. Spin-polarized local density approximation (LDA) [18] with the Perdew–Zunger parameterization of the Ceperley–Alder (CA) Monte Carlo correlation data was used to approximate the exchange–correlation functional. To maintain consistency, the PAW potentials were generated using the same CA-LDA functional. A kinetic energy cutoff of 500 eV was applied, and the electronic self-consistent energy convergence criterion was set to 10^{-8} eV. Structural optimizations were carried out until the Hellmann–Feynman forces on each atom were less than 0.001 eV/Å. The Brillouin zone was sampled using a $18 \times 18 \times 5$ k -point mesh. To accurately capture vdW interactions, the DFT-D3 dispersion correction scheme was employed [19, 20].

III. RESULTS and DISCUSSION

We begin by optimizing the crystal structure of Fe₃GaTe₂ under hydrostatic pressure using first-principles DFT calculations [21]. Fe₃GaTe₂ crystallizes in a layered hexagonal structure with space group $P6_3/mmc$ (No. 194). As illustrated in Figs. 1(a) and 1(b), the conventional unit cell contains two formula units (f.u.) and comprises two weakly coupled slabs stacked along the crystallographic c -axis, held together by vdW interactions. Each slab consists of five atomic sublayers: Te atoms occupy the top and bottom layers, Fe_I atoms are situated in the second and fourth layers, and the central layer hosts both Fe_{II} and Ga atoms. Within each sublayer, the atoms form 2D triangular lattices. In particular, three Te atoms at the corners of a triangle bond with a single Fe_I atom positioned at the triangle’s hollow site, forming a characteristic local coordination geometry. Meanwhile, Ga atoms occupy

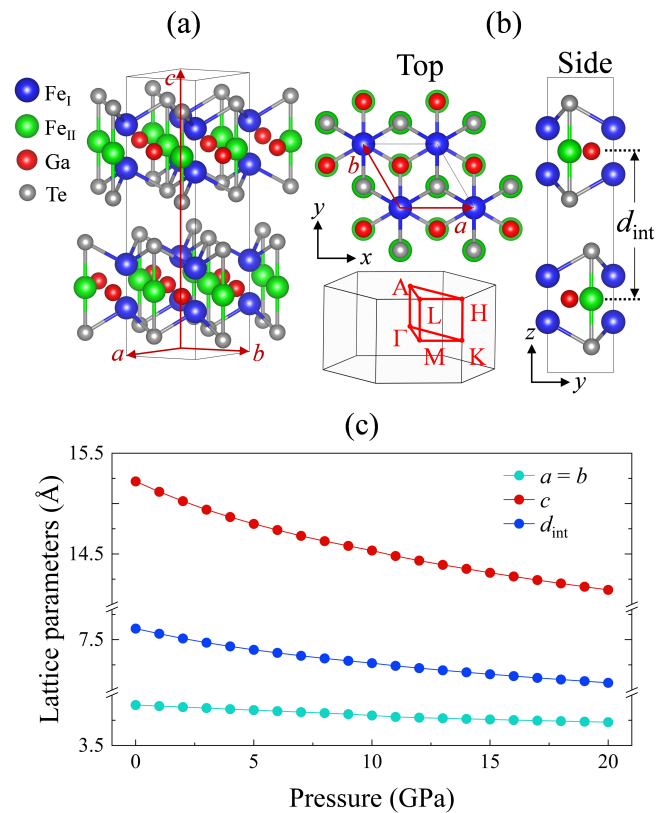


FIG. 1. Optimized crystal structure of Fe₃GaTe₂: (a) Perspective view of the layered structure; (b) top and side views of the unit cell, together with the first Brillouin zone of the hexagonal lattice; (c) calculated pressure dependence of the lattice parameters a , b , and c , as well as the interlayer spacing d_{int} . The lattice parameters are $a = (a, 0, 0)$, $b = (-b \sin(30^\circ), b \cos(30^\circ), 0)$, and $c = (0, 0, c)$ in the x, y, z coordinate system.

the in-plane hollow sites coordinated by the Fe_{II} sublattice. This arrangement results in a specific trilayered Fe₃Ga framework sandwiched between two Te layers, yielding a quasi-2D structure. Upon full structural relaxation, the optimized lattice constants at zero pressure are found to be $a = b = 3.901$ Å and $c = 15.221$ Å, with an interlayer spacing of $d_{\text{int}} = 2.677$ Å (see Table I). Figure 1(c) shows the pressure dependence of the lattice parameters a , b , and c , as well as d_{int} . While all structural parameters decrease monotonically with increasing pressure, the compressibility along the c -axis is significantly greater than in the in-plane directions, resulting in a more pronounced reduction in c and d_{int} compared to a and b . This anisotropic structural response reflects the intrinsic softness of the vdW gap under pressure.

Figure 2(a) shows the spin-polarized band structure and local density of states (LDOS) of ferromagnetic Fe₃GaTe₂ at zero pressure, calculated using the LDA functional without SOC. The electronic states near E_F are primarily derived from the Fe $3d$ orbitals of both Fe_I and Fe_{II}. The band structure exhibits hole-like dispersions along the Γ – A direction and electron-like bands along K – H . The overall dispersions along

TABLE I. Calculated lattice parameters a , b , c , and interlayer spacing d_{int} of Fe_3GaTe_2 at zero pressure [22], in comparison with previous theoretical [23] and experimental [5, 24, 25] results. The employed exchange-correlation functionals, including CA-LDA and the generalized gradient approximation functional of Perdew, Burke, and Ernzerhof (PBE-GGA) [28], are indicated in parentheses.

	a (Å)	b (Å)	c (Å)	d_{int} (Å)
Present (CA-LDA)	3.901	3.901	15.221	2.677
Present (PBE-GGA)	4.032	4.019	16.109	2.887
Previous theory (PBE-GGA) [23]	4.034	4.034	16.090	
Experiment [5]	3.986	3.986	16.229	
Experiment [24]	3.970	3.970	15.560	
Experiment [25]	4.090	4.090	16.070	

high-symmetry paths such as Γ - M , Γ - K , A - L , and A - H are consistent with previous DFT study and angle-resolved photoemission spectroscopy (ARPES) measurements [25, 29]. Figure 2(b) displays the calculated Fermi surface (FS) contours at $k_z = 0$ and $k_z = \pi/c$. At $k_z = 0$, the FS contains multiple hole pockets centered at Γ , including outer hexagonal contours, along with several triangular-like electron pockets at the K points, reflecting the threefold rotational symmetry of the lattice. In contrast, at $k_z = \pi/c$, the FS shows moderate reconstruction: five hole pockets encircle A , and two triangular-like electron pockets appear at the H points. The FS variation at $k_z = \pi/c$ arises from the non-symmorphic nature of the $P6_3/mmc$ space group, which enforces double degeneracy of all bands at $k_z = \pi/c$ in each spin channel. The band dispersion along the Γ - A direction, as shown in Fig. 2(a), reflects finite interlayer dispersion along the c -axis, which originates from weak vdW interactions between adjacent layers. Notably, both occupied and unoccupied states at the M and L points give rise to van Hove singularities (VHSs) near E_F , resulting in prominent LDOS peaks. In particular, the occupied states generate VHS1 and VHS2 at the M point, located at -0.318 and -0.448 eV below E_F , and VHS3 at the L point, located at -0.386 eV [see Fig. 2(a)]. These features align well with the strong ARPES intensity distributed between -0.3 and -0.5 eV at the same momenta [25]. Therefore, the LDA-derived electronic structure reliably captures both the FS topology and VHS-related LDOS features, providing a solid foundation for analyzing the pressure-induced evolution of electronic and magnetic properties in Fe_3GaTe_2 .

To investigate how the electronic structure evolves under pressure, we present the pressure-dependent LDOS of Fe_I , Fe_{II} , and Te atoms over a broad energy range [see Figs. 3(a)-3(c)]. With increasing pressure, all atomic species exhibit noticeable band broadening, indicating enhanced orbital hybridization. Notably, the LDOS of Te shows a systematic expansion of the band edges, denoted by E_{min} and E_{max} , with pressure [see Fig. 3(c)]. The values of E_{min} (E_{max}) are -6.586 (5.690), -6.818 (5.874), -7.000 (6.018), -7.188 (6.147), and -7.355 (6.275) eV at 0, 5, 10, 15, and 20 GPa, respectively. The LDOS peaks of Fe_I and Fe_{II} appear at similar energies, suggesting strong hybridization between the two

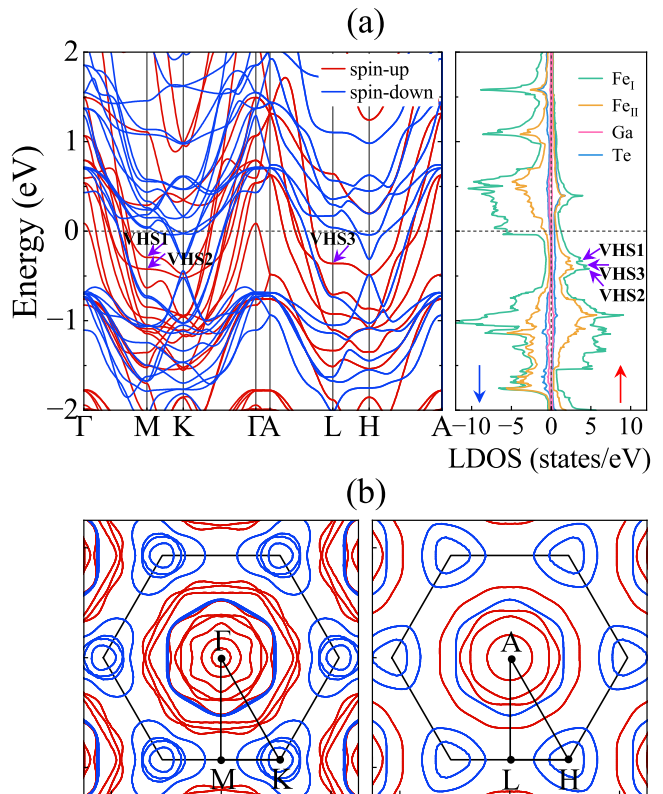


FIG. 2. (a) Calculated spin-polarized band structure of Fe_3GaTe_2 at zero pressure, along with the LDOS projected onto the Fe_I , Fe_{II} , and Te atoms. The VHS1, VHS2, and VHS3 are marked in the band structure and LDOS in panel (a). The red and blue arrows represent the spin-up and spin-down LDOS, respectively. The LDOS is given in units of states/eV per f.u. (b) Corresponding FS contours in the $k_z = 0$ (left) and $k_z = \pi/c$ (right) planes.

Fe sublattices, likely mediated by Te p orbitals. In addition to the overall broadening, the LDOS near E_F exhibits spin-dependent energy shifts with increasing pressure [see arrows in Figs. 3(a) and 3(b)]: spin-up states shift upward, while spin-down states shift downward. This behavior reduces the exchange splitting and causes a redistribution of spectral weight from spin-up to spin-down channels, leading to a net suppression of spin polarization.

To clarify the orbital character of the states indicated by the arrows in Fig. 3, we have included the partial density of states (PDOS) for Fe_I , Fe_{II} , Te , and Ga atoms near E_F in Supplemental Fig. S2 [26]. For the spin-up states (indicated by maroon arrows), the dominant contributions come from the Fe_I d_{z^2} orbital and the Fe_{II} d_{xz}/d_{yz} orbitals. In contrast, the spin-down states (indicated by cyan arrows) involve Fe_I d_{xz}/d_{yz} and Fe_{II} d_{z^2} orbitals. The comparable spectral weight of the spin-up states on Fe_I and Fe_{II} suggests strong hybridization between Fe_I d_{z^2} and Fe_{II} d_{xz}/d_{yz} orbitals. For the spin-down states, the corresponding PDOS peaks in Te/Ga p orbitals indicate hybridizations between Fe_I d_{xz}/d_{yz} and Te/Ga p_z orbitals, as well as between Fe_{II} d_{z^2} and Ga p_x/p_y orbitals. These differ-

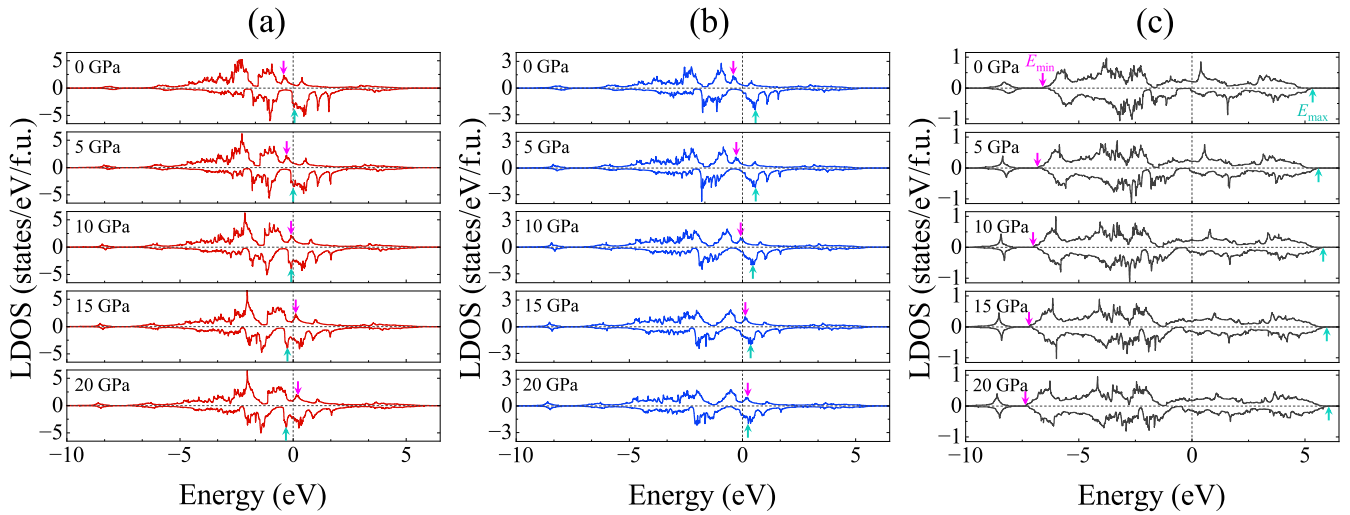


FIG. 3. Calculated pressure-dependent LDOS for (a) Fe_I , (b) Fe_{II} , and (c) Te atoms. The arrows in panels (a) and (b) highlight the LDOS peaks near E_F . The maroon (cyan) arrows for the spin-up (spin-down) states in panels (a) and (b) highlight the LDOS peaks near E_F . In panel (c), the arrows indicate the lower (E_{\min}) and upper (E_{\max}) band edges, corresponding to the occupied and unoccupied states, respectively.

ent orbital hybridizations between Fe and Te/Ga atoms, where the $\text{Fe}_I/\text{Te}(\text{Ga})$ interaction involves p_z (out-of-plane) orbitals and the Fe_{II}/Ga interaction involves p_x/p_y (in-plane) orbitals, may be associated with the divergent pressure responses of the MAE for Fe_I/Te and Fe_{II} , as discussed below.

Figure 4 displays the pressure dependence of the magnetic moments for Fe_I and Fe_{II} . At zero pressure, Fe_I has a larger magnetic moment than Fe_{II} possibly due to a more prominent unoccupied spin-down LDOS just above E_F , as shown in Fig. 2. The magnetic moment on Te remains negligible ($< \sim 0.05 \mu_B$), indicating that magnetism is primarily localized on the Fe sublattices. As pressure increases up to 10 GPa, both Fe sites show a pronounced reduction in magnetic moment (see Fig. 4). For Fe_I , this is primarily due to the downward shift of spin-down states located just above E_F , which become partially occupied as they move below the Fermi level. Additionally, spin-up states near E_F shift upward and become depopulated, further contributing to the decline in spin polarization. A similar mechanism applies to Fe_{II} , resulting in a simultaneous drop in moment. Beyond 10 GPa, the rate of moment reduction slows markedly, and the magnetic moments of Fe_I and Fe_{II} gradually converge. This crossover reflects more subtle, nonuniform changes in the band structure near E_F , and marks the onset of saturation in spin-state redistribution. Notably, this regime coincides with the emergence of magnetic anisotropy switching, which will be discussed below. The numbers in Fig. 4 show the spin-resolved Fe d -electron counts for both Fe_I and Fe_{II} sites as a function of pressure, illustrating how the d -orbital occupations evolve and correlate with the pressure-induced reduction in magnetic moments. Collectively, these results underscore the itinerant nature of magnetism in Fe_3GaTe_2 . The continuous and pressure-tunable variation of magnetic moments, driven by changes in the electronic structure near E_F , is a characteristic feature of

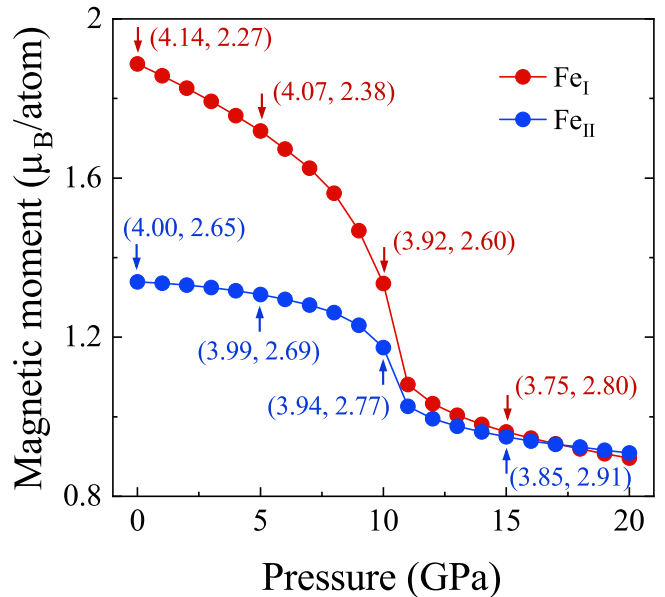


FIG. 4. Calculated pressure dependence of the spin magnetic moments of Fe_I and Fe_{II} . The paired numbers in parentheses represent the spin-up and spin-down Fe d -electron counts, respectively.

itinerant ferromagnetism in layered vdW materials.

Next, we investigate the MAE of Fe_3GaTe_2 by including SOC [30]. The MAE is defined as the total energy difference between in-plane and out-of-plane magnetization directions, i.e., $\text{MAE} = E_{\parallel} - E_{\perp}$, where E_{\parallel} and E_{\perp} denote the total energies for in-plane and out-of-plane magnetizations, respectively. In this convention, a positive MAE indicates an out-of-plane magnetic easy axis, while a negative value corresponds to an in-plane one. As shown in Fig. 5(a), the MAE at zero pressure is positive, with a value of 0.677 meV/f.u.,

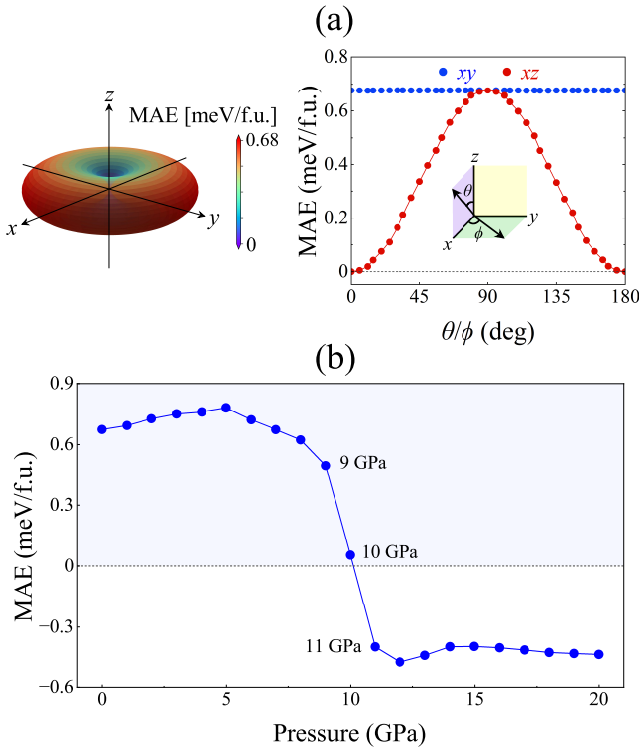


FIG. 5. (a) Calculated MAE of Fe_3GaTe_2 at zero pressure, along with its angular dependence in the xz and xy planes as a function of the angles θ and ϕ , respectively. (b) Pressure dependence of the MAE.

indicating that the easy axis lies along the c -axis. Figure 5(b) shows the pressure dependence of the MAE. With increasing pressure, the MAE varies weakly before decreasing, and ultimately changes sign near 10 GPa, indicating a pressure-driven spin reorientation from an out-of-plane to an in-plane easy axis. This behavior is consistent with recent experimental observations [14]. Notably, this critical pressure for MAE sign reversal coincides with a pronounced drop in the magnetic moments of Fe_I and Fe_{II} (see Fig. 4), reflecting a common microscopic origin. The reorientation is likely driven by pressure-induced modifications in the spin-resolved electronic states near E_F : occupied spin-up bands shift upward, while unoccupied spin-down bands move downward (see Fig. 3). These opposing shifts lead to high LDOS peaks associated with Fe_I and Fe_{II} crossing E_F , resulting in a redistribution of spin-resolved occupations. The subsequent reduction of local magnetic moments alters the SOC interactions, ultimately reversing the MAE sign. These results demonstrate that the MAE in Fe_3GaTe_2 is highly sensitive to pressure-driven evolution of the electronic structure near E_F , as will be discussed below.

To elucidate the microscopic origin of the pressure-induced switching of the magnetic easy axis in Fe_3GaTe_2 , we analyze the atom- and orbital-resolved contributions to the MAE at 9, 10, and 11 GPa, as shown in Fig. 6. This decomposition reveals that the dominant driving forces behind the MAE

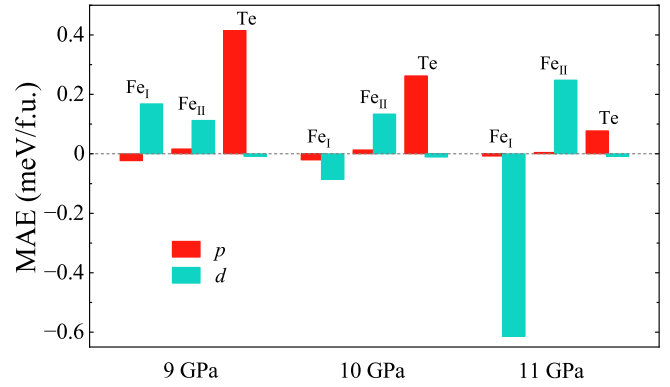


FIG. 6. Calculated atom- and orbital-resolved contributions to the MAE in Fe_3GaTe_2 at 9, 10, and 11 GPa.

sign reversal arise from the Fe_I and Te atoms. Specifically, the MAE contributions from Fe_I (Te) are +0.145 (+0.407), -0.106 (+0.252), and -0.622 (+0.069) meV/f.u. at 9, 10, and 11 GPa, respectively, indicating that both atoms together ultimately drive the sign change in the total MAE under pressure. In contrast, the contribution from Fe_{II} increases monotonically with pressure, amounting to 0.129, 0.147, and 0.253 meV/f.u. at the respective pressures. Despite this positive contribution, it is insufficient to counterbalance the increasingly negative contributions from Fe_I and Te, resulting in a net reduction and eventual reversal of the total MAE near 10 GPa [see Fig. 5(b)]. Consequently, the magnetic easy axis reorients from out-of-plane to in-plane. These findings indicate that the spin reorientation is primarily governed by pressure-induced modifications in the spin-orbit interaction of Fe_I and Te atoms, which exhibit markedly different behavior from that of Fe_{II} , as further discussed below.

Figures 7(a)–7(c) present a detailed orbital-resolved decomposition of the MAE at 9 GPa, illustrating interorbital coupling contributions from Fe_I , Fe_{II} , and Te atoms. For Fe_I d orbitals, three major channels are identified: a negative contribution from the $(d_{xy}, d_{x^2-y^2})$ pair, and two positive contributions from the (d_{xz}, d_{yz}) and (d_{yz}, d_{z^2}) pairs [Fig. 7(a)]. In contrast, Fe_{II} exhibits moderate positive contributions from the $(d_{xy}, d_{x^2-y^2})$ and (d_{xz}, d_{yz}) pairs, while the (d_{yz}, d_{z^2}) pair contributes negatively [Fig. 7(b)]. These SOC interactions yield an overall positive MAE from both Fe sites, with Fe_I contributing slightly more, consistent with Fig. 6. For the Te p orbitals, the MAE originates from the (p_x, p_y) and (p_y, p_z) channels, both contributing positively [Fig. 7(c)]. The lower panels of Figs. 7(a)–7(c) show the evolution of these interorbital contributions from 9 to 11 GPa. Notably, the MAE contributions from Fe_I and Te decrease with pressure and become negative in several channels, indicating a substantial suppression of their magnetic anisotropy. Meanwhile, the contributions from Fe_{II} remain nearly constant or increase slightly, reinforcing the conclusion that the pressure-induced spin reorientation is mainly governed by changes in the MAE contributions from Fe_I and Te.

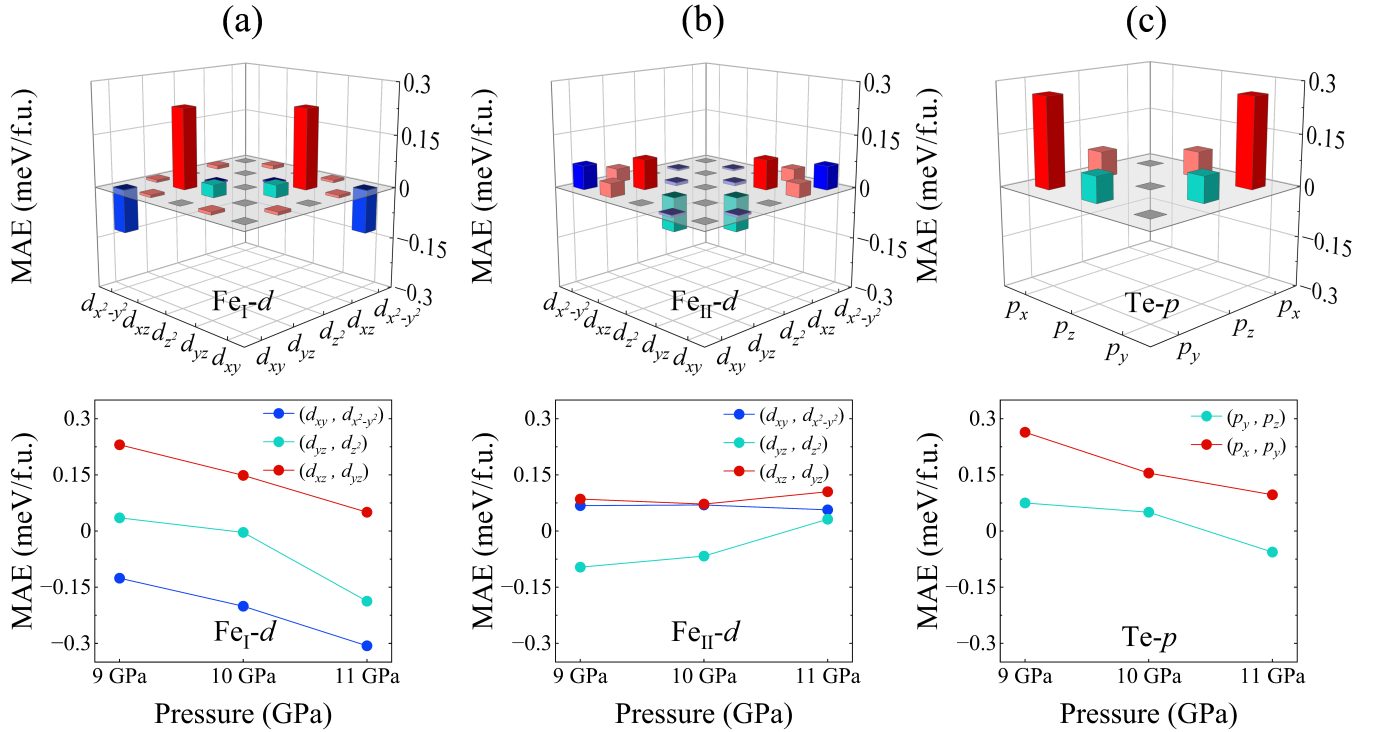


FIG. 7. Interorbital contributions to the MAE from (a) $\text{Fe}_I d$, (b) $\text{Fe}_{II} d$, and (c) $\text{Te } p$ orbitals at 9 GPa. The lower panels show the evolution of these contributions with increasing pressure from 9 to 11 GPa. Positive (negative) values correspond to a preference for out-of-plane (in-plane) magnetic anisotropy.

It is worth noting that second-order perturbation theory is formally applicable to systems with discrete and well-separated energy levels, such as insulators or semiconductors [31–33]. In metallic systems like Fe_3GaTe_2 , however, its applicability is limited due to strong band hybridization, partial orbital occupancies, and frequent band crossings near E_F . These features complicate a strictly quantitative interpretation of SOC-induced magnetic anisotropy. Nevertheless, the contrasting pressure dependence of orbital-resolved MAE contributions from Fe_I , Fe_{II} , and Te atoms can be qualitatively understood by considering their distinct local environments and the effects of anisotropic lattice strain. Under hydrostatic compression, the lattice contracts more significantly along the c -axis than within the ab plane [see Fig. 1(c)], resulting in effective uniaxial strain along the out-of-plane direction. This anisotropic deformation modifies the local crystal field and orbital hybridization in a site- and orbital-dependent manner. Fe_I and Te atoms, positioned near the vdW gap, are particularly sensitive to interlayer spacing. As pressure reduces this spacing, the spatial extent and overlap of $\text{Fe}_I d$ and $\text{Te } p$ orbitals—especially those with out-of-plane character—are significantly altered. These changes can suppress SOC matrix elements that favor out-of-plane anisotropy or enhance those contributing to in-plane anisotropy, leading to a reduction and eventual sign reversal of their MAE contributions under pres-

sure [see Figs. 6, 7(a), and 7(c)]. In contrast, Fe_{II} atoms are embedded within the interior Fe – Ga layer, where they are coordinated predominantly in-plane and are less directly influenced by interlayer compression. However, pressure can still modify their in-plane crystal field environment and orbital overlap. Such changes may suppress in-plane SOC contributions or amplify those favoring out-of-plane anisotropy, leading to the gradual increase in the Fe_{II} MAE contribution under pressure, as shown in Figs. 6 and 7(b). The divergent pressure responses of Fe_I/Te and Fe_{II} reflect the interplay between their distinct bonding environments and orbital characteristics. While Fe_I and Te respond strongly to interlayer interactions and out-of-plane lattice contraction, Fe_{II} , residing in a more symmetric and covalently bonded in-plane network, exhibits a contrasting trend. These findings underscore the importance of anisotropic lattice strain and local orbital geometry in modulating SOC-driven magnetic anisotropy in layered metallic systems. Despite the inherent limitations of perturbation theory in itinerant metallic systems, the present analysis offers a physically consistent and insightful interpretation of the pressure-dependent MAE evolution in Fe_3GaTe_2 .

IV. SUMMARY

Our first-principles calculations for Fe_3GaTe_2 revealed a magnetic easy-axis transition from out-of-plane to in-plane at a critical pressure of approximately 10 GPa, in good agreement with experimental observations [14]. Around this pressure, pressure-induced electronic band broadening leads to a substantial reduction in magnetization. Notably, the SOC contributions to the MAE exhibit distinct site-dependent behavior. The Fe_I and Te atoms near the vdW gap experience enhanced interlayer interactions, which suppress their out-of-plane anisotropy and eventually favor in-plane spin alignment. In contrast, the central Fe_{II} atoms in the Fe–Ga layer show a modest enhancement of out-of-plane preference under pressure; however, this is insufficient to counterbalance the dominant in-plane contributions from Fe_I and Te. This contrast in site-resolved SOC responses accounts for the observed easy-axis switching. Our findings highlighted the interplay between electronic band evolution and site-specific SOC effects under pressure in tuning magnetic anisotropy, and demonstrated pressure as a powerful means of controlling spin orientation in layered metallic ferromagnets.

ACKNOWLEDGEMENTS

This work was supported by the Natural Science Foundation of Henan (No. 252300421216), the talent Introduction Project in Henan Province (HNGD2025008), the Innovation Program for Quantum Science and Technology (No. 2021ZD0302800), the International Cooperation Project of Science and Technology of Henan Province (No. 242102520029), and the Foundation of Henan Educational Committee (No. 25A140003). J.H.C acknowledges the support from the National Research Foundation of Korea (NRF) grant funded by the Korean Government (Grant No. RS202300218998). The calculations were performed by the KISTI Supercomputing Center through the Strategic Support Program (Program No. KSC-2024-CRE-0055) for the super-computing application research.

J. L. and S. L. contributed equally to this work.

* Corresponding authors: wb@henu.edu.cn and cho@henu.edu.cn

DATA AVAILABILITY

The data that support the findings of this article are not publicly available. The data are available from the authors upon reasonable request.

[1] B. Huang, G. Clark, E. Navarro-Moratalla, D. R. Klein, R. Cheng, K. L. Seyler, D. Zhong, E. Schmidgall, M. A. McGuire and D. H. Cobden, Layer-dependent ferromagnetism in a van

der Waals crystal down to the monolayer limit, *Nature*, **546**, 270 (2017).

[2] C. Gong, L. Li, Z. Li, H. Ji, A. Stern, Y. Xia, T. Cao, W. Bao, C. Wang and Y. Wang, Discovery of intrinsic ferromagnetism in two-dimensional van der Waals crystals, *Nature*, **546**, 265 (2017).

[3] Z. Fei, B. Huang, P. Malinowski, W. Wang, T. Song, J. Sanchez, W. Yao, D. Xiao, X. Zhu and A. F. May, Two-dimensional itinerant ferromagnetism in atomically thin Fe_3GeTe_2 , *Nat. Mater.*, **17**, 778 (2018).

[4] M. Ribeiro, G. Gentile, A. Marty, D. Dosenovic, H. Okuno, C. Vergnaud, J.-F. Jacquot, D. Jalabert, D. Longo and P. Ohresser, Large-scale epitaxy of two-dimensional van der Waals room-temperature ferromagnet Fe_5GeTe_2 , *npj 2D Mater. Appl.*, **6**, 10 (2022).

[5] G. Zhang, F. Guo, H. Wu, X. Wen, L. Yang, W. Jin, W. Zhang and H. Chang, Above-room-temperature strong intrinsic ferromagnetism in 2D van der Waals Fe_3GaTe_2 with large perpendicular magnetic anisotropy, *Nat. Commun.*, **13**, 5067 (2022).

[6] M. Bonilla, S. Kolekar, Y. Ma, H. C. Diaz, V. Kalappattil, R. Das, T. Eggers, H. R. Gutierrez, M.-H. Phan and M. Batzill, Strong room-temperature ferromagnetism in VSe_2 monolayers on van der Waals substrates, *Nat. Nanotechnol.*, **13**, 289 (2018).

[7] D. J. O'Hara, T. Zhu, A. H. Trout, A. S. Ahmed, Y. K. Luo, C. H. Lee, M. R. Brenner, S. Rajan, J. A. Gupta and D. W. McComb, Room temperature intrinsic ferromagnetism in epitaxial manganese selenide films in the monolayer limit, *Nano Lett.*, **18**, 3125 (2018).

[8] B. Li, Z. Wan, C. Wang, P. Chen, B. Huang, X. Cheng, Q. Qian, J. Li, Z. Zhang and G. Sun, Van der Waals epitaxial growth of air-stable CrSe_2 nanosheets with thickness-tunable magnetic order, *Nat. Mater.*, **20**, 818 (2021).

[9] X. Zhang, Q. Lu, W. Liu, W. Niu, J. Sun, J. Cook, M. Vaninger, P. F. Miceli, D. J. Singh and S.-W. Lian, Room-temperature intrinsic ferromagnetism in epitaxial CrTe_2 ultrathin films, *Nat. Commun.*, **12**, 2492 (2021).

[10] Y. Deng, Y. Yu, Y. Song, J. Zhang, N. Z. Wang, Z. Sun, Y. Yi, Y. Z. Wu, S. Wu and J. Zhu, Gate-tunable room-temperature ferromagnetism in two-dimensional Fe_3GeTe_2 , *Nature*, **563**, 94 (2018).

[11] H. Wang, H. Lu, Z. Guo, A. Li, P. Wu, J. Li, W. Xie, Z. Sun, P. Li and H. Damas, Interfacial engineering of ferromagnetism in wafer-scale van der Waals Fe_4GeTe_2 far above room temperature, *Nat. Commun.*, **14**, 2483 (2023).

[12] W. Du, M. Liu, F. Han, H. Su, H. Zhang, B. Liu, H. Meng and X. Tang, Role of oxygen migration on the thermal stability of the perpendicular magnetic anisotropy in bottom and top structures, *APL Mater.*, **10**, 011101 (2022).

[13] X.-Q. Wang, Y.-W. Geng, Z. Wang, C. Xie, T. Han and P. Cheng, Two-Dimensional Metal–Organic Framework with High-Performance Single-Molecule Magnets as Nodes Showing Magnetic Coercivity Photomodulation, *J. Am. Chem. Soc.*, **147**, 18044 (2025).

[14] X. Gao, K. Zhai, H. Fu, J. Yan, D. Yue, F. Ke, Y. Zhao, C. Mu, A. Nie and J. Xiang, F. Wen, B. Wang, T. Xue, L. Wang, H. Yuan, and Z. Liu, Enhanced Ferromagnetism and Tunable Magnetic Anisotropy in a van der Waals Ferromagnet, *Adv. Sci.*, **11**, 2402819 (2024).

[15] G. Kresse and J. Hafner, Ab initio molecular dynamics for open-shell transition metals, *Phys. Rev. B*, **48**, 13115 (1993).

[16] G. Kresse and J. Furthmüller, Efficiency of ab-initio total energy calculations for metals and semiconductors using a plane-wave basis set, *Comput. Mater. Sci.*, **6**, 15 (1996).

[17] P. E. Blöchl, Projector augmented-wave method, *Phys. Rev. B*,

- 50, 17953 (1994).
- [18] J. P. Perdew and A. Zunger, Self-interaction correction to density-functional approximations for many-electron systems, *Phys. Rev. B*, **23**, 5048 (1981); D. M. Ceperley and B. J. Alder, Ground State of the Electron Gas by a Stochastic Method, *Phys. Rev. Lett.* **45**, 566 (1980).
- [19] S. Grimme, J. Antony, S. Ehrlich, and H. Krieg, A Consistent and Accurate ab initio Parametrization of Density Functional Dispersion Correction (DFT-D) for the 94 Elements H-Pu, *J. Chem. Phys.*, **132**, 154104 (2010).
- [20] S. Grimme, S. Ehrlich, and L. Goerigk, Effect of the Damping Function in Dispersion Corrected Density Functional Theory, *J. Comput. Chem.*, **32**, 1456 (2011).
- [21] For the application of hydrostatic pressure, we perform enthalpy minimization with both the cell shape and volume relaxed at each pressure.
- [22] We note that the CA-LDA structural parameters are underestimated compared to the present and previous [23] PBE-GGA calculations and experimental results [5, 24, 25]. However, as will be shown later, the CA-LDA functional are in better agreement with the experimental magnetic moments in Fe_3GaTe_2 compared to the PBE-GGA functional (see Supplemental Table S1 [26]). Additionally, while CA-LDA shows a pronounced reduction in the magnetic moment around 10 GPa (see Fig. 4), PBE-GGA predicts a magnetic-moment drop at higher pressures, around 40 GPa (see Supplemental Fig. S1 [26]).
- [23] Y. Xu, X. Jin, J. Xiang, H. Zhang and F. Tian, DFT+ DMFT investigation of the magnetic phase transition in the itinerant ferromagnet Fe_3GaTe_2 , *Phys. Rev. B*, **111**, 155142 (2025).
- [24] R. Iimori, S. Hu, A. Mitsuda and T. Kimura, Substantial enhancement of perpendicular magnetic anisotropy in van der Waals ferromagnetic Fe_3GaTe_2 film due to pressure application, *Commun. Mater.*, **5**, 235 (2024).
- [25] J.-E. Lee, S. Yan, S. Oh, J. Hwang, J. D. Denlinger, C. Hwang, H. Lei, S.-K. Mo, S. Y. Park and H. Ryu, Electronic structure of above-room-temperature van der Waals ferromagnet Fe_3GaTe_2 , *Nano Lett.*, **23**, 11526 (2023).
- [26] See Supplemental Material at <http://link.aps.org/supplemental/xx.xxxx> for the pressure dependence of magnetic moments under PBE-GGA functional, the PDOS for Fe_I , Fe_{II} , Te, and Ga atoms near E_F , and the comparison of magnetic moments between calculations [27] and experiments.
- [27] A. M. Ruiz, D. L. Esteras, D. López-Alcalá and J. J. Baldoví, On the origin of the above-room-temperature magnetism in the 2D van der Waals ferromagnet Fe_3GaTe_2 , *Nano Letters* **24**, 7886 (2024).
- [28] J. P. Perdew, K. Burke, and M. Ernzerhof, Generalized Gradient Approximation Made Simple, *Phys. Rev. Lett.* **77**, 3865 (1996); **78**, 1396 (1997).
- [29] H. Zha, W. Li, G. Zhang, W. Liu, L. Deng, Q. Jiang, M. Ye, H. Wu, H. Chang and S. Qiao, Enhanced Magnetic Interaction between Ga and Fe in Two-Dimensional van der Waals Ferromagnetic Crystal Fe_3GaTe_2 , *Chin. Phys. Lett.*, **40**, 087501 (2023).
- [30] All MAE calculations were performed with SOC included, which enables the noncollinear formalism in VASP. The magnetization directions were controlled by specifying the global spin quantization axis using the SAXIS tag and appropriately setting the initial MAGMOM values. This setup allowed for a direct comparison between in-plane and out-of-plane orientations. The Tetrahedron method with Blöchl corrections was used for the integration without smearing, which is crucial for accurate results in metals. As the k -mesh increases to $28 \times 28 \times 7$, the calculated MAE changes by less than a few $\mu\text{eV}/\text{f.u.}$, confirming that the $18 \times 18 \times 5$ k -mesh used in our calculations is sufficiently converged.
- [31] B. Wang, Y. Bai, C. Wang, S. Liu, S. Yao, Y. Jia, J. Cho, Ferroelectric control of magnetic anisotropy in multiferroic heterostructure $\text{EuSn}_2\text{As}_2/\text{In}_2\text{Se}_3$, *Phys. Rev. B*, **110**, 094423 (2024).
- [32] J. Zhang, Y. Shao, C. Li, J. Xu, H. Zhang, C. Wang, B. Wang, J. Cho, Nonvolatile electrical control of magnetic anisotropy in ferromagnetic LaBr_2 monolayer on ferroelectric In_2Se_3 substrate, *Appl. Phys. Lett.*, **125**, 142404 (2024).
- [33] Q. Cui, Y. Zhu, J. Jiang, J. Liang, D. Yu, P. Cui, and H. Yang, Ferroelectrically controlled topological magnetic phase in a Janus-magnet-based multiferroic heterostructure, *Phys. Rev. Res.*, **3**, 043011 (2021).